ELSEVIER

Earth and Planetary Science Letters 182 (2000) 93–101

EPSL

www.elsevier.com/locate/epsl

Large-scale lateral heat and fluid transport in the seafloor: revisiting the well-mixed aquifer model

N.D. Rosenberg [a,*], A.T. Fisher [b,c], J.S. Stein [b]

[a] *Earth and Environmental Sciences Directorate, Lawrence Livermore National Laboratory, Livermore, CA 94551, USA*
[b] *Earth Sciences Department, University of California, Santa Cruz, CA 95064, USA*
[c] *Institute of Tectonics, University of California, Santa Cruz, CA 95064, USA*

Received 14 December 1999; accepted 27 July 2000

Abstract

Large-scale, lateral fluid flow through oceanic crust provides an explanation for regionally low heat flow in several seafloor settings. A well-mixed aquifer (WMA) model provides a quantitative and conceptual tool for explaining anomalously low heat flow based on an analytical representation of fluid and heat flow, assuming lateral fluid flow in basement in a layer directly below the ocean sediments. We present an extended well-mixed aquifer (EWMA) model that allows fluid flow at greater depths within the oceanic crust. Flow through a deeper permeable layer extracts more heat than equivalent flow through a shallower layer of equal thickness, and may help to reconcile global heat flow and seafloor permeability data, since deeper flow does not require velocities as great as shallow flow to account for the same heat loss, and thus permeability can be lower. Numerical simulations that test the hydrodynamic validity of the WMA and EWMA equations indicate that the analytical models provide reasonable approximations of large-scale, lateral heat transport when lateral fluid flow in the crust is confined to thin layers. The efficiency of lateral heat transport is reduced as vertical mixing within the lateral flow layer increases.

Keywords: ocean floors; hydrothermal conditions; heat flow; fluid dynamics

1. Introduction

Thermally driven circulation of seawater through the oceanic crust profoundly influences the physical, chemical, and biological evolution of the crust and the oceans. While considerable attention has been focused on hot springs along the mid-ocean ridge axis, global advective heat loss from ridge flanks (crust older than one million years) is three times that at the axis [1], and the ridge flank mass flux is at least 10 times that at the axis [2]. Hydrothermal exchange between crust and oceans lasts tens of millions of years and affects more than one-third of the ocean floor, generating solute fluxes of several elements similar in magnitude to those of riverine and ridge crest sources, and extensively altering oceanic basement [3,4].

Conductive models for cooling lithosphere [1,5–7] provide a reference to which observations of seafloor heat flow can be compared. The global heat flow deficit (deviation from the conductive

* Corresponding author.

0012-821X/00/$ – see front matter
PII: S0012-821X(00)00235-1

lithosphere model) is thought to result from advective heat loss that cannot be measured using conventional heat flow instrumentation. For oceanic crust younger than 65 Ma, the deficit is about $11 \pm 4 \times 10^{12}$ W, or $34 \pm 12\%$ of oceanic heat flow, and most of this deficit is accumulated on ridge flanks, in crust older than 1 Ma [8]. Large-scale, lateral fluid flow through oceanic basement can mine heat efficiently from the crust and explain the heat flow deficit.

The heat flow deficit for crust younger than 65 Ma requires that enormous fluid fluxes recharge, flow laterally, and discharge from oceanic basement. Lateral fluid flow is the key to efficient extraction of lithospheric heat because relatively impermeable sediments prevent thermally significant, vertical fluid flow from the crust to the ocean except at widely spaced, narrow discharge zones (i.e., faults, basement outcrops). The nature of such lateral flows and the driving forces that sustain them remain poorly understood.

The well-mixed aquifer (WMA) model was introduced to explain anomalously low seafloor heat flow in the Brazil Basin [9], and has subsequently been applied in other settings [10–12] and to the global heat flow data set [13]. The WMA model is one-dimensional mathematically, but two-dimensional in concept. Cold seawater enters a permeable layer in upper basement and warms while flowing laterally until it discharges at the seafloor (Fig. 1A). Fluid is assumed to be well mixed so that there is no vertical temperature gradient within the zone of lateral fluid flow. Heat flow through the sediments overlying basement is conductive. Lithospheric heat flow into the base of the crust (q_0) depends only on crustal age, but heat flow at the seafloor (q_x) is greatly reduced near the recharge area, and increases with distance from the recharge area, eventually reaching the lithospheric value (Fig. 1B). The observed heat flow fraction (q_x/q_0) depends on the physical properties of sediment and basement, the rate of lateral fluid flow, and distance from the area of recharge.

The WMA model requires that fluid flow is restricted to uppermost basement beneath the sediments, but seafloor borehole logs and experiments demonstrate that permeable zones within oceanic crust are not always so restricted (e.g., [14–16]). Faults and other tectonized zones could allow large-scale fluid flow within deeper crustal levels but the WMA model cannot represent these features. In addition, when the WMA model was introduced, it was noted that "[t]he aquifer model is an *ad hoc* one that explains the geothermal observations and is not derived from fundamental hydrodynamic principles" ([9], p. 10817]. Subsequent numerical models have used a conductive proxy for vigorous mixing during lateral flow in oceanic basement [17,18], but it is not clear if this approximation is hydrodynamically reasonable, nor how local mixing influences the efficiency of lateral heat advection.

In this report, we review the assumptions inherent in the WMA model and derive a modified version that relaxes the requirement for lateral fluid flow to occur only within uppermost basement, allowing us to test the potential significance of lateral flow below uppermost basement for global heat flow and permeability data sets. We then assess the hydrodynamic validity of these analytical results through comparison with two-dimensional, coupled heat and fluid flow numerical simulations. The analytical models are idealizations and are not intended to represent the complications associated with specific settings (i.e., basement relief, variable sediment thickness, flow in and out of a two-dimensional cross-section, multiple flow layers), but they are useful for quickly assessing lateral flow associated with heat flow suppression. More sophisticated analyses require detailed numerical modeling, including site-specific geometries and properties.

2. Original well-mixed aquifer model

The WMA model is based on a one-dimensional, steady-state, heat balance equation:

$$hk_h \frac{d^2T}{dx^2} - hv\rho c \frac{dT}{dx} - q_x + q_0 = 0 \quad (1)$$

where x = horizontal distance, T = temperature of fluid within lateral flow layer (aquifer), v = specific

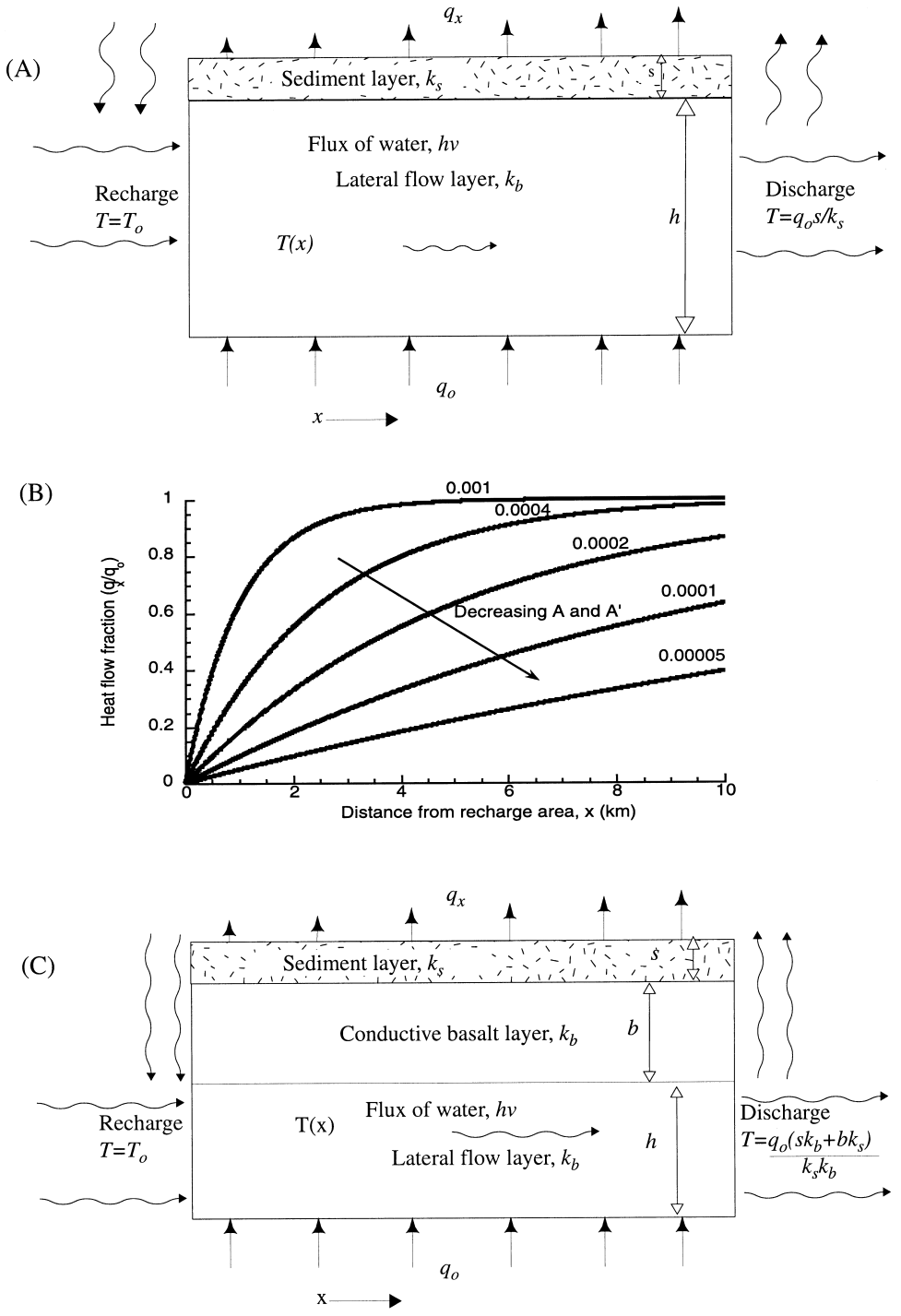

Fig. 1. (A) Cartoon of the WMA model (modified from [9]). (B) Heat flow fraction (q_x/q_0) as a function of distance from the recharge area using different values of $A=k_s/hscv\rho$. The same curves apply to the EWMA model using $A'=(k_b k_s)/(sk_b+bk_s)\cdot(1/hcv\rho)$ rather than A. (C) Cartoon of EWMA model.

discharge (Darcy velocity), k_h = thermal conductivity of the lateral flow layer, h = thickness of the lateral flow layer, c = heat capacity of the water, and ρ = density of the water (Fig. 1A). Seafloor heat flow is defined as:

$$q_x = k_s T/s \tag{2}$$

where s = sediment thickness, k_s = sediment thermal conductivity, the seafloor temperature is 0°C, and q_0 is the basal heat flow. An analytical solution to Eq. 1, assuming $T(x_0) = 0$°C, and $q_x(\infty) = q_0$ is [9]:

$$q_x/q_0 = 1-\exp\left[x\left(\beta/2-\sqrt{(\beta^2/4 + k_s/k_h hs)}\right)\right] \tag{3}$$

where:

$$\beta = v\rho c/k_h$$

If the first term in Eq. 1 (conduction) is assumed to be small relative to the second term in Eq. 1 (advection), Eq. 3 is reduced to [11]:

$$q_x/q_0 = 1-\exp(-Ax) \tag{4}$$

where:

$$A = k_s/hscv\rho$$

This solution results in greater advective heat loss for a lateral flow layer having greater thickness, for higher lateral fluid velocities, and for a deeper permeable layer (i.e., thicker sediments) (Fig. 1B).

3. Extended well-mixed aquifer model

We propose an extended well-mixed aquifer (EWMA) model that allows for conductive sediment and conductive (impermeable) basement above a permeable basement layer (Fig. 1C). We define q_x in terms of the conductive heat transport through the combined sediment/basement conductive layer:

$$q_x = \frac{T}{(s/k_s) + (b/k_b)} = T(k_s k_b)/(sk_b + bk_s) \tag{5}$$

where b = thickness of the conductive basement layer and k_b = thermal conductivity of this layer. The new solution to Eq. 1 following application of Eq. 5 and other conditions as before is:

$$q_x/q_0 = 1-\exp(-A'x) \tag{6}$$

where:

$$A' = (k_b k_s)/(sk_b + bk_s)\cdot(1/hcv\rho)$$

Calculations based on Eq. 6 are still represented by the curves in Fig. 1B, but A is replaced by A'. This approach could be expanded to included additional conductive layers.

We apply the EWMA model to extend the analyses of Fisher and Becker [13], in which they used the WMA model to estimate large-scale crustal permeabilities required to explain the global heat flow anomaly over young crust. Fisher and Becker [13] linked the global heat flow data set to crustal permeability through a combination of Eq. 4 and Darcy's law, which relates the specific discharge to permeability, viscosity and pressure gradients driving large-scale lateral flow. Pressure gradients were estimated based on the difference in fluid density between downflow and upflow zones. The lateral fluid flux required to explain the mean heat flow fraction as a function of age [1] was then used in combination with the available driving forces to calculate the minimum necessary crustal permeability, given different thicknesses of the lateral flow and sediment layers, and spacing between recharge and discharge sites that increases with crustal age. Results of these calculations suggest that large-scale crustal permeabilities must be high, in the order of 10^{-12}–10^{-7} m^2 in seafloor younger than 10 Ma, to allow lateral fluid fluxes great enough to explain the observed heat flow fraction (q_x/q_0). In contrast, sparse borehole permeability data from uppermost basement suggest that bulk permeability decreases from 10^{-10} to 10^{-13} m^2 within the first 3–4 Ma of crustal evolution [19].

In a new set of calculations, we reconsider two of the cases examined previously [13]: (1) h = 100 m and a sedimentation rate = 5 m/Myr and (2) h = 100 m and a sedimentation rate of 50 m/Myr.

Sediment thickens as the crust ages, and the distance between entry and exit points for hydrothermal fluids is assumed to increase with age as Δx (km) = 5.0+0.5 × age (Ma). In the original calculations, the lateral flow layer was directly below the deepest sediments, equivalent to the EWMA model with $b = 0$ m. We calculate minimum permeabilities (and associated fluid fluxes) that allow a match to the observed heat flow fraction at a point midway between entry and exit points, for lateral flow layers at different depths below the top of the basement–sediment interface (Fig. 2). For a given layer thickness and fluid flux, a deeper lateral flow layer extracts more heat than a shallower layer, because it is assumed in the model that the water enters the lateral flow layer at bottom-water temperature. There is a greater initial temperature contrast for a deeper layer, and heat flow suppression is greater. The assumption that fluid enters the lateral flow layer at bottom-water temperature results in the largest possible lateral pressure gradient, and thus the lowest possible permeability.

Deeper layers allow slower lateral fluid velocities to match the observed heat flow fraction, and thus permeability can be lower by several orders of magnitude compared to flow immediately below the sediments, depending on the assumed depth of flow. In addition, the available driving force for large-scale lateral flow increases as the depth of the lateral flow layer increases, because deeper flow requires taller columns of recharge and discharge fluid. Several of the curves in Fig. 2 suggest that minimum bulk permeability values initially increase as the crust ages. This is most likely to occur for flow layers deep within the crust where the driving forces for lateral flow do not fall as rapidly as the lateral flow rate necessary to explain the observed heat flow suppression in the global data set. The curves in Fig. 2 are not intended to represent the permeability of oceanic crust along an aging path; instead, they indicate the minimum permeability required for a given set of conditions necessary to explain the global heat flow pattern based on the EWMA model. Only under unusual circumstances might permeability increase as the crust ages, for example, where the crust is flexed at the swell outboard of a subduction zone.

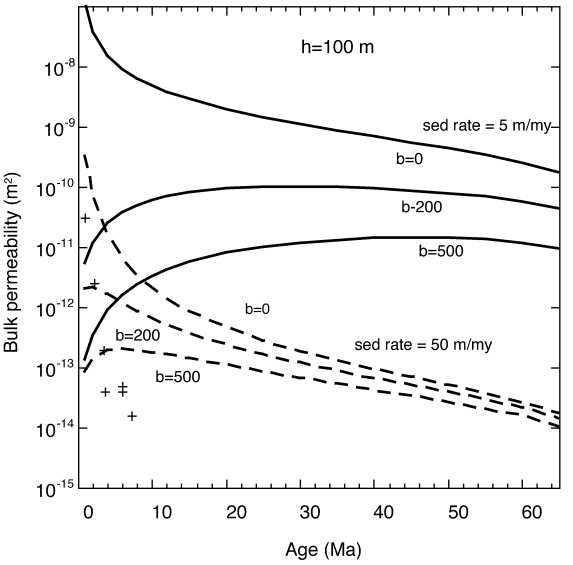

Fig. 2. Crustal-scale bulk permeability required by observed seafloor heat flow fraction, based on the EWMA model and Darcy's law. Analysis modified from [13]. The lateral flow layer was assumed to be 100 m thick and was located at various depths below the sediment–basement interface, as labeled. The EWMA with $b = 0$ m is equivalent to the WMA model. Sedimentation rates shown were used to calculate basement depth as a function of crustal age, and the distance between recharge and discharge sites was assumed to increase linearly, as described in the text. Borehole permeability values [19] are plotted with '+' for reference.

The crustal scale permeabilities estimated using the EWMA model are still greater than most direct measurements [16,19], but the match is closer for deeper permeable layers than for shallow permeable layers of equal thickness. For a permeable layer 500 m below the basement–sediment interface, large-scale crustal permeabilities need to be of the order of 10^{-13}–10^{-11} m^2 (Fig. 2), rather than 10^{-12}–10^{-7} m^2 for a permeable layer directly below the sediments [13]. We note that a deeper lateral flow layer presents some practical difficulties since bottom seawater must penetrate to depth at the recharge area, and move rapidly to the seafloor at the discharge area, and any energy lost during vertical fluid motion would not be available to drive lateral flow.

Reconciling the differences between measured and modeled permeability values is complicated by many factors, including variations in measurement methods and assumptions, and the possibility that borehole permeability measurements tend to miss highly permeable channels in the extrusive layers [13,16]. Very few borehole measurements of permeability in oceanic crust have been made below the uppermost extrusive section, and values tend to decrease rapidly below the upper few hundred meters [16]. One set of borehole measurements in a gabbroic crustal section in the Indian Ocean revealed relatively high permeability within a restricted, tectonized zone [15], but the lateral extent of this feature, and its relation to the unique environment close to a fracture zone, is unclear. Listric normal faulting (e.g., [20–23]) could create subhorizontal permeable zones deep within oceanic crust, but the frequency and lateral extent of such zones remain to be quantified.

4. Hydrogeologic models of lateral flow aquifer

We performed a series of two-dimensional numerical simulations of systems similar to those described above to evaluate whether the WMA or EWMA models are hydrodynamically reasonable representations of advective heat transport in oceanic crust. Simulations were performed using the finite-element code FEHM [24], with modifications to the fluid properties subroutines to allow a larger range of pressures and temperatures. Cold fluid was forced to enter at one end of a uniform horizontal layer below conductive sediment and basement, and exit at the other end of the horizontal layer at a constant specific discharge, after being warmed by heat flow from below (Fig. 3A). As in the WMA and EWMA models, vertical flow at recharge and discharge sites is assumed to be adiabatic, so that heat is exchanged only as the fluid flows laterally. Temperature- and pressure-dependent fluid properties (i.e., density, heat capacity) vary as the water flows laterally, and a combination of conduction and advection occurs within the lateral flow layer.

In the first set of simulations, we impose laminar flow conditions through use of horizontal anisotropy in permeability to test how well the WMA and EWMA models simulate conditions with no vertical mixing. Results of numerical simulations agree well with both the WMA and the EWMA models when the lateral flow layers are thin, but the solutions diverge for thicker lateral flow layers. Numerical and analytical results are compared in Fig. 3B, which shows q_x/q_0 versus x curves for two cases for which the WMA solutions are identical. In the thin layer case ($s = 50$ m, $h = 40$ m, $v = 10^{-7}$ m/s), the WMA and FEHM solutions agree well. In the thick layer case ($s = 50$ m, $h = 400$ m, $v = 10^{-8}$ m/s), agreement between the WMA and FEHM solutions is poorer. Because the WMA and EWMA models are nonlinear, the definition of 'thin' and 'thick' varies for different values of A and A'. In the FEHM two-dimensional simulations, the discharge temperature increases approximately linearly from the top of the lateral flow layer to the bottom of that layer. The difference between the average temperature in the lateral flow layer and that at

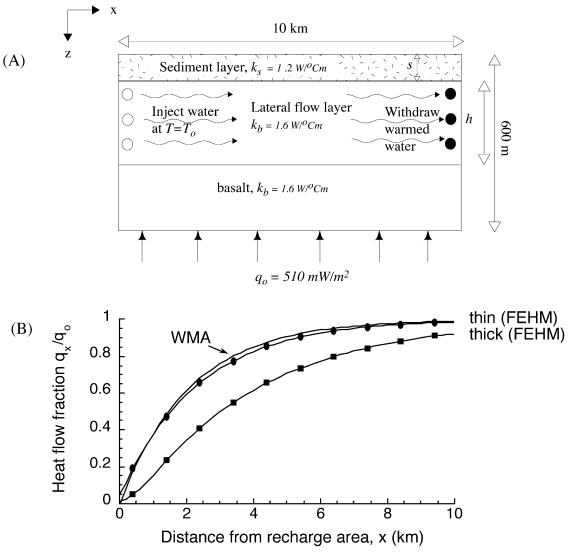

Fig. 3. (A) Model configuration for two-dimensional numerical simulations for partially coupled heat and fluid flow within ocean crust. Grid cells were 200 m (horizontal) by 20 m (vertical). (B) Comparison of analytical and numerical solutions with no vertical mixing. The WMA analytical solution (solid line, no symbols) is identical for the two cases: a thin layer ($s = 50$ m, $h = 40$ m, $v = 10^{-7}$ m/s) and a thick layer ($s = 50$ m, $h = 400$ m, $v = 10^{-8}$ m/s).

the top of the layer increases with layer thickness. Because the WMA and EWMA models are based on a one-dimensional lateral flow layer, there is a single value for discharge temperature.

Next, we considered the 400 m lateral flow layer modeled previously, but with high isotropic permeability that permits vertical mixing. The overall flux of fluid through the lateral flow layer is the same for cases with and without vertical mixing. Temperature fields are shown in Fig. 4A–C, and a plot of q_x/q_0 versus x for these cases is shown in Fig. 4D. The anisotropic case (Fig. 4A) represents pure forced convection, with no vertical mixing. Two isotropic cases (Fig. 4B,C) are in the mixed convection regime, a combination of forced convection and free convection. The permeability in the first case (Fig. 4B) is two orders of magnitude greater than the permeability in the second case (Fig. 4C). Convective cells begin to form in the first case close to the recharge area, creating a more vertically homogeneous temperature field, enhancing vertical heat transport, and substantially reducing heat suppression due to lateral flow as compared to the case with no vertical mixing (Fig. 4A). In the lower permeability case (Fig. 4C), forced convection dominates close to the recharge area. In this region, heat flow is significantly suppressed and little vertical mixing occurs. Convection cells form farther from the recharge area where q_x/q_0 is near one. For a given horizontal distance from the recharge zone, there is a trade-off between degree of vertical mixing and magnitude of heat flow suppression (Fig. 4D). Lateral flow in a layer with some vertical mixing can result in measurable heat flow suppression (Fig. 4D), but the lateral flux through the layer would need to increase to result in the same heat flow suppression as the case with no vertical mixing.

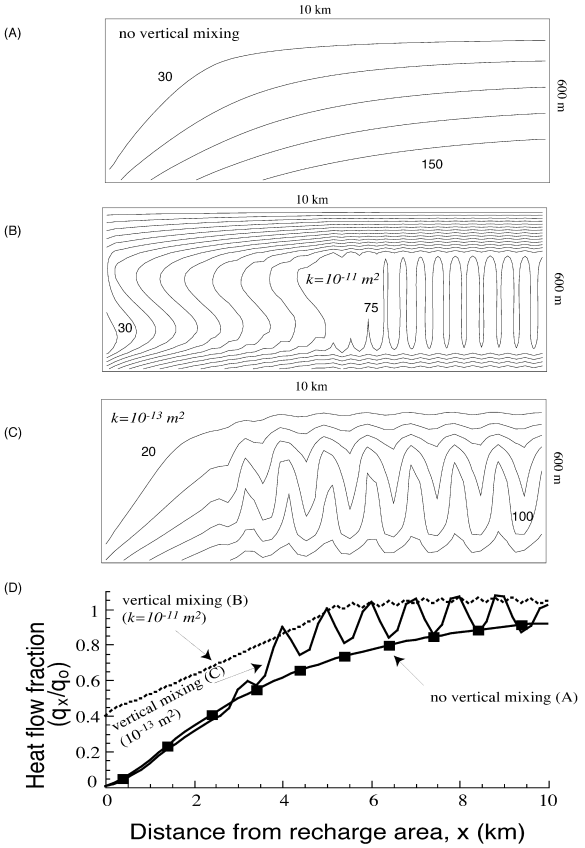

Fig. 4. Numerical results for coupled heat and fluid flow in a two-dimensional system with the same lateral fluid fluxes. (A) Temperature field for numerical solution of large-scale lateral flow in a 400 m thick layer with no vertical mixing (same 400 m layer case as shown in Fig. 3B). Temperature contour interval is 30°C. (B) Temperature field for the same case but with vertical mixing allowed; isotropic permeability in lateral flow layer is 10^{-11} m^2, and temperature contour interval is 5°C. Because the system is allowed to convect freely it is thermally more homogeneous than in the case with no vertical mixing. (C) Temperature field for the same case, but with isotropic permeability in lateral flow layer of 10^{-13} m^2. Temperature contour interval is 20°C. Convection still occurs, but mixing is less vigorous than in the case with higher permeability. (D) Heat flow fraction (q_x/q_0) as a function of distance from the recharge area for all three cases. The case with no vertical mixing is most efficient in suppressing seafloor heat flow, and the case with the most vigorous vertical mixing is the least efficient in suppressing seafloor heat flow.

5. Conclusions

The original WMA model provides a quantitative and conceptual understanding of thermal transport based on a one-dimensional representation of fluid and heat flow, but is limited to lateral fluid flow in a basement layer directly below the sediments. The EWMA model is based on many of the same assumptions, but allows fluid flow at a greater depth within the oceanic crust. Flow through a deeper permeable layer may extract

more heat than flow through an equivalent shallower layer, and may help to reconcile the observed heat flow and seafloor permeability data, provided there is a way to move recharging and discharging fluids vertically without significant energy loss. This requires that vertical conduits have very high permeability, since driving forces in ridge flanks are limited, and that these conduits be well connected to lateral flow layers at depth. Whether such deep, permeable layers are common in the oceanic crust remains to be determined through direct measurement.

Numerical simulations of coupled heat and fluid flow indicate that WMA and EWMA analytical solutions are good approximations of large-scale lateral heat transport when lateral fluid flow in the crust occurs in thin layers. The analytical models are less appropriate as the lateral flow layer thickens. The thermal efficiency of lateral heat transport (as expressed by low values of q_x/q_0 away from the recharge site) is reduced as vertical mixing within the lateral flow layer increases. This result has implications for the high Nusselt number approximation used to simulate efficient vertical and lateral mixing in the presence of large-scale lateral flow, since these two processes are coupled, and an increase in vertical mixing results in less efficient lateral heat transport.

Acknowledgements

This manuscript benefitted greatly from reviews by R. Carlson, R. Harris, and an anonymous reviewer. This research was supported by the Los Alamos National Laboratory Visiting Scholar Program (STB-UC96-136), NSF OCE-9819252, and CULAR (LANL/UCSC) project STB-UC98-181. ***[EB]***

References

[1] C.A. Stein, S. Stein, Constraints on hydrothermal heat flux through the oceanic lithosphere from global heat flow, J. Geophys. Res. 99 (1994) 3081–3095.

[2] M.J. Mottl, C.G. Wheat, Hydrothermal circulation through mid-ocean ridge flanks: Fluxes of heat and magnesium, Geochim. Cosmochim. Acta 58 (1994) 2225–2237.

[3] J. Alt, Sulfur isotopic profile through the oceanic crust – sulfur mobility and seawater–crustal sulfur exchange during hydrothermal alteration, Geology 23 (1995) 585–588.

[4] H. Elderfield, A. Schultz, Mid-ocean ridge hydrothermal fluxes and the chemical composition of the ocean, Annu. Rev. Earth Planet. Sci. 24 (1996) 191–224.

[5] B. Parsons, J.G. Sclater, An analysis of the variation of ocean floor bathymetry and heat flow with age, J. Geophys. Res. 82 (1977) 803–827.

[6] E.E. Davis, C.R.B. Lister, Heat flow measured over the northern Juan de Fuca Ridge: evidence for widespread hydrothermal circulation in a highly heat-transportive crust, J. Geophys. Res. 83 (1977) 4845–4860.

[7] C.A. Stein, S. Stein, A model for the global variation in oceanic depth and heat flow with lithospheric age, Nature 359 (1992) 123–129.

[8] C.A. Stein, S. Stein, A.M. Pelayo, Heat flow and hydrothermal circulation, in: S.E. Humphris, R.A. Zierenberg, L.S. Mullineaux, R.E. Thompson (Eds.), Seafloor Hydrothermal Systems: Physical, Chemical, Biological and Geological Interactions, AGU Geophys, Monogr, 91 (1995) 425–445.

[9] M.G. Langseth, B.M. Herman, Heat transfer in the oceanic crust of the Brazil Basin, J. Geophys. Res. 86 (1981) 10805–10819.

[10] M.G. Langseth, K. Becker, R.P. Von Herzen, P. Schultheiss, Heat and fluid flux through sediment on the western flank of the Mid-Atlantic Ridge: A hydrogeological study of North Pond, Geophys. Res. Lett. 19 (1992) 517–520.

[11] M.G. Langseth, R.D. Hyndman, K. Becker, S.H. Hickman, M.H. Salisbury, The hydrogeological regime of isolated sediment ponds in mid-oceanic ridges, Init. Rep. DSDP 78B (1984) 825–837.

[12] P.A. Baker, P.M. Stout, M. Kastner, H. Elderfield, Large-scale lateral advection of seawater through oceanic crust in the central equatorial Pacific, Earth Planet. Sci. Lett. 105 (1991) 522–533.

[13] A.T. Fisher, K. Becker, Channelized fluid flow in oceanic crust reconciles heat-flow and permeability data, Nature 403 (2000) in press.

[14] M. Matthews, M. Salisbury, R. Hyndman, Basement logging on the Mid-Atlantic Ridge, Deep Sea Drilling Project Hole 395A, Init. Rep. DSDP 78B (1984) 717–730.

[15] K. Becker, In-situ bulk permeability of oceanic gabbros in Hole 735B, ODP leg 118, Proc. ODP Sci. Results 118 (1991) 333–347.

[16] A.T. Fisher, Permeability within basaltic oceanic crust, Rev. Geophys. 36 (1998) 143–182.

[17] E.E. Davis, D.S. Chapman, K. Wang, H. Villinger, A.T. Fisher, S.W. Robinson, J. Grigel, D. Pribnow, J. Stein, K. Becker, Regional heat flow variations across the sedimented Juan de Fuca Ridge eastern flank: Constraints on lithospheric cooling and lateral hydrothermal heat transport, J. Geophys. Res. 104 (1999) 17675–17688.

[18] E.E. Davis, K. Wang, J. He, D.S. Chapman, H. Villinger, A. Rosenberger, An unequivocal case for high Nusselt number hydrothermal convection in sediment-buried igneous oceanic crust, Earth Planet. Sci. Lett. 146 (1997) 137–150.

[19] K. Becker, A.T. Fisher, Permeability of upper oceanic basement on the eastern flank of the Juan de Fuca Ridge determined with drill-string packer experiments, J. Geophys. Res. 105 (2000) 897–912.

[20] M.H. Salisbury, C.E. Keen, Listric faults imaged in oceanic crust, Geology 21 (1993) 117–120.

[21] S. Agar, K. Klitgord, A mechanism for decoupling within the oceanic lithosphere revealed in the Troodos ophiolite, Nature 374 (1995) 232–238.

[22] G. Guerin, K. Becker, R. Gable, P. Pezard, Temperature measurements and heat-flow analysis in Hole 504B, Proc. ODP Sci. Results (1996) 291–296.

[23] J.A. Karson, Internal structure of oceanic lithosphere: a perspective from tectonic windows, in: W.R. Buck, P.T. Delaney, J.A. Karson, Y. Lagabrielle (Eds.), Faulting and Magmatism at Mid-Ocean Ridges, AGU Geophys. Monogr. 106 (1998) 177–218.

[24] G.A. Zyvoloski, B.A. Robinson, Z.V. Dash, L.L. Trease, Models and Methods Summary for the FEHMN Application, Los Alamos National Laboratory Report LA-UR-94-3788, Rev. 1, 1995.